Available online at www.sciencedirect.com
SCIENCE DIRECT
International Journal of Heat and Fluid Flow 27 (2006) 611–618
International Journal of HEAT AND FLUID FLOW
www.elsevier.com/locate/ijhff

# An experimental study on turbulent swirling water flow with immiscible droplets

Takuro Kouda, Yoshimichi Hagiwara *

*Department of Mechanical and System Engineering, Kyoto Institute of Technology, Goshokaido-cho, Matsugasaki, Sakyo-ku, Kyoto 606-8585, Japan*

Available online 17 April 2006

**Abstract**

Measurements have been carried out for the turbulent swirling water flow with low-density immiscible silicon-oil droplets in a horizontal pipe. An impeller fixed inside the pipe generates the swirl, which is stronger than that in our previous study. The flow is visualized with fluorescent tracer particles, which are captured with video cameras from the side and downstream end of the pipe. The instantaneous velocity field is obtained from the captured images with the particle tracking velocimetry method. The results indicate that the size and motion of the droplets depends on the buoyancy force, lift force, pressure-gradient force and drag force. It is considered that the increase in the turbulence intensity is due to the wake flow of the droplets.


*Keywords:* Horizontal pipe flow; Oil droplets; Swirl; Turbulence modification

## 1. Introduction

It is believed that the recovery of waste heat is promising to reduce global warming. The amount of waste heat in warm water from houses, hotels and factories is not negligible. Thus, it is necessary to develop efficient methods of heat transfer for the recovery of this kind of waste heat.

Direct-contact heat transfer between the water flow (continuous-phase flow) and immiscible droplets (dispersed phase) is found from the following points to meet this requirement: (1) heat loss due to walls separating one liquid from another is minimized, and (2) the heat transfer surface increases by many small droplets. Therefore, this direct-contact heat transfer has been studied widely in the last two decades. Lee (1987) measured the overall heat transfer coefficient and the size distribution of droplets in the liquid–liquid two-phase flow. Jacobs and Golafshani (1989) demonstrated that the circulation inside the immiscible droplets enhanced heat transfer in their large-scale apparatus. Kaviany (1994) summarized the interaction between an immiscible droplet and its surrounding flow. Mitrovic and Stephan (1996) discussed equations for mean temperatures for the direct-contact heat exchange without evaporation. Inaba et al. (1998) obtained empirical equations for heat transfer and the size distribution of the immiscible droplets in the water flow. The droplets were transported in the central regions of the flows in these studies, and the heat of one phase was transferred efficiently to the other phase in these regions.

In the case of small-scale distributed heat exchangers for factories, hotels and houses, flows with immiscible droplets in passages in vertical and horizontal directions should be considered. Our group showed that the immiscible droplets of low specific weight in turbulent downward water flow in a duct approached the duct wall far from the injection nozzle of droplets (Hagiwara et al., 2005). We also exhibited that the immiscible droplets of high specific weight in turbulent upward water flow approached the wall (Hagiwara et al., 2003). In the case of horizontal flows, the droplets, whose density is different from that of water, are transported to the wall due to buoyancy force or gravitational force. Furthermore, two adjacent droplets should be far enough so that the heat transfer from/to ambient liquid to/from the

* Corresponding author. Tel.: +81 75 724 7324; fax: +81 75 724 7300.
*E-mail address:* yoshi@kit.ac.jp (Y. Hagiwara).

0142-727X/$ - see front matter © 2006 Elsevier Inc. All rights reserved.
doi:10.1016/j.ijheatfluidflow.2006.02.022

**Nomenclature**

| | |
|---|---|
| $D$ | pipe diameter |
| $d$ | droplet equivalent diameter |
| $d_p$ | particle diameter |
| $g$ | gravitational acceleration |
| $l_K$ | Kolmogorov length scale |
| $N$ | number of frames which include the droplet images |
| $Re_D$ | Reynolds number |
| $Re_d$ | droplet Reynolds number |
| $r$ | radial distance |
| $St$ | Stokes number defined by Eq. (2) |
| $Sw$ | Swirl number defined by Eq. (1) |
| $V_m$ | bulk mean velocity |
| $V_r$ | radial mean velocity |
| $V_z$ | streamwise mean velocity |
| $V_\theta$ | azimuthal mean velocity |
| $V_{\theta max}$ | maximum value of the time-averaged azimuthal velocity |
| $v_{rel}$ | instantaneous relative velocity between droplet and surrounding flow |
| $v'_{zrms}$ | root-mean square value of fluctuating streamwise velocity |
| $v_\tau$ | friction velocity |
| $x$, $y$, $z$ | distances in the horizontal, vertical and streamwise directions |
| $x_0$, $y_0$ | position of the center of particle |
| $\varepsilon$ | dissipation rate of turbulent kinetic energy |
| $\mu$ | water viscosity |
| $\nu$ | water kinematic viscosity |
| $\rho$ | water density |
| $\rho_d$ | droplet density |
| $\rho_p$ | particle density |
| $\sigma$ | interfacial tension |
| $\tau_d$ | characteristic time of droplet |
| $\tau_f$ | characteristic time of swirl |

droplet is not attenuated by the motion of another droplet. Therefore, the control of the path of droplets being transported in the different types of flow is highly desirable to maintain efficient heat transfer between the phases.

We have considered that adding rotation to the main flow is effective for the attenuation of the wallward motion of the droplets. Magaud et al. (2003) carried out their experimental and theoretical study on swirling water flow with bubbles in a vertical pipe. However, their results are not available to predict the flow characteristics of the horizontal turbulent swirling flow with immiscible droplets. Thus, we carried out an experiment on the turbulent swirling water flow with silicon-oil droplets in a horizontal pipe and obtained the result that many droplets were transported along the axis in a specific region. Also, we discussed the turbulence modification due to the droplets (Kouda and Hagiwara, 2006).

In the present study, we measure the droplets motion and flow turbulence in the case of a stronger swirl than that in our previous study and discuss the force balance acting on the droplets and turbulence modification due to the droplets. Furthermore, the experimental procedure is improved so that the phase interface is identified clearly.

## 2. Apparatus

### 2.1. Test loop

The apparatus is shown schematically in Fig. 1. This apparatus is the same as that in our previous study (Kouda and Hagiwara, 2006) except for the impeller. The water loop consists of an upstream chamber, a contraction nozzle, a horizontal pipe made of acrylic resin (with an inner diameter $D$ of 50 mm), an elbow with a window, a downstream chamber, a pump and connecting tubes. The length of the pipe was 3050 mm (=61$D$). A tripping wire was placed on the inner surface at the inlet of the pipe in order to promote turbulence. The water flow rate was controlled by an inverter connected to the pump. The Reynolds number based on $D$, the bulk mean velocity $V_m$ and the kinematic viscosity $\nu$, $Re_D = V_m D/\nu$, was $3.6 \times 10^3$. This Reynolds number is approximately 35% lower than that in our previous study (Kouda and Hagiwara, 2006).

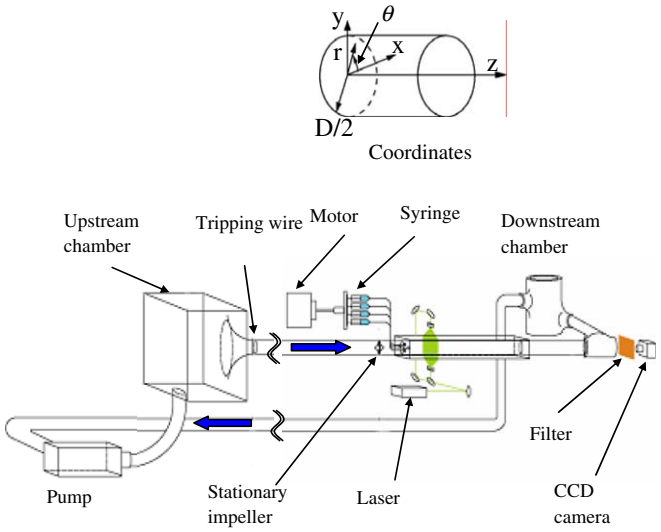


Fig. 1. Schematic diagram of apparatus.

### 2.2. Impeller

Since the swirl observed in our previous study (Kouda and Hagiwara, 2006) was weak, we replaced the impeller.

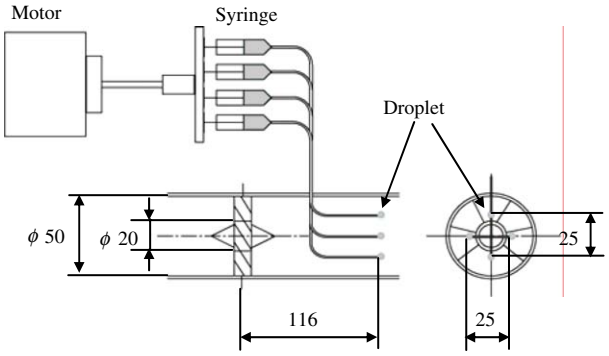


Fig. 2. Details of impeller and droplet injection tubes. Dimensions in mm.

The blades of the new impeller are bigger than those of the previous one. The new impeller was fixed at 2110 mm (=42.2$D$) from the inlet of the horizontal pipe where the velocity field was developed. The detail of the impeller is shown in Fig. 2. The origin of the coordinates was defined at the center of the impeller. The $x$, $y$ and $z$ coordinate axes were positioned in a horizontal direction, a vertical direction and a streamwise direction, respectively. The test section was set in the region of $115 < z < 715$ mm ($2.3D < z < 14.3D$).

In order to estimate the effect of swirl on the main flow at a specific cross section, the swirl number defined by the following equation (Kitoh, 1991) was used:

$$Sw(z) = \frac{2\pi \int_0^{D/2} V_\theta(r,z) V_z(r,z) r^2 \, \mathrm{d}r}{\pi (D/2)^3 V_m^2}, \tag{1}$$

where $V_\theta(r,z)$ and $V_z(r,z)$ are the mean velocities in the azimuthal and streamwise directions, respectively, and $r = \sqrt{x^2 + y^2}$ is the radial coordinate. This swirl number is the ratio of the momentum due to the swirl at the cross section and the momentum transported downstream.

### 2.3. Immiscible droplets

Silicon oil (KF995, Shin-Etsu Chemical Co., Ltd.) was adopted as the fluid of the immiscible droplets. The physical properties of this oil are shown in Table 1. The interfacial tension in this table was measured with the Wilhelmy plate method by using a surface tensiometer (Kyowa Interface Science Co. Ltd., CBVP-Z).

The silicon oil was injected simultaneously from four fine stainless-steel tubes, whose inner diameter was 0.8 mm (see Fig. 2). The outlets of these tubes were located at $(0.25D, 0, 2.3D)$, $(0, 0.25D, 2.3D)$, $(-0.25D, 0, 2.3D)$ and $(0, -0.25D, 2.3D)$. Each tube was connected to a syringe. All the syringes were pushed at a constant speed so that the volumetric flow rates of oil in the tubes were identical. The ratio of the total volumetric flow rate of oil to that of main water flow was 0.0036. The oil injected from the tube outlets did not form columns but formed droplets intermittently. The oil droplets carried by the water flow were collected at the exit of the downstream chamber.

The Stokes number defined by the following equation (Tanaka et al., 2003) was introduced in order to analyze the droplet motion:

$$St = \frac{\tau_\mathrm{d}}{\tau_\mathrm{f}} = \frac{2\rho_\mathrm{d} + \rho}{36\mu} d^2 \Big/ \frac{D}{V_{\theta\max}}, \tag{2}$$

where $\tau_\mathrm{d}$ is the characteristic time of a droplet, $\tau_\mathrm{f}$ is the characteristic time of the swirl, $\rho_\mathrm{d}$ is the droplet density, $\rho$ is the water density, $\mu$ is the water viscosity, $d$ is the droplet equivalent diameter and $V_{\theta\max}$ is the maximum value of the time-averaged azimuthal velocity. The Stokes number depends only on the droplet diameter because $V_{\theta\max}$ is constant.

## 3. Flow visualization

The flow was visualized with the fluorescent tracer particles, which were made by adsorbing Rhodamine B to the particles. The specific weight of the particle, $\rho_\mathrm{p}/\rho$, was 1.02. The diameter of these particles $d_\mathrm{p}$ was in the range of 0.053–0.075 mm. $d_\mathrm{p}$ was approximately 0.15–0.36 times larger than the Kolmogorov length scale, $l_\mathrm{K}$, calculated by the following equation:

$$l_\mathrm{K} = \left(\nu^3/\varepsilon\right)^{1/4} = \nu \Big/ \left((\varepsilon^+)^{1/4} v_\tau\right), \tag{3}$$

where $\varepsilon$ is the dissipation rate of turbulent kinetic energy, $\varepsilon^+$ is its non-dimensional form and $v_\tau$ is the friction velocity. $v_\tau$ was estimated from the mean value of the wall shear stress, which was calculated from the mean velocity distributions both in the streamwise and the azimuthal directions. The value of $\varepsilon^+$ was in the range of 0.02–0.16 depending on the distance from the pipe axis according to the results of direct numerical simulation carried out by Satake and Kunugi (1998).

How much the particles follow sinusoidal liquid motion was examined based on the result obtained by Hjelmfelt and Mockros (1966). The upper limit of the frequency, beyond which the ratio of the amplitude for the particle motion to that of the sinusoidal liquid motion becomes less than 0.99, was estimated to be higher than 533 Hz. This

Table 1
Physical properties

| | Water | KF995 |
|---|---|---|
| Specific weight | 1 | 0.96 |
| Kinematic viscosity (mm$^2$/s) | 1.0 | 4.0 |
| Interfacial tension (mN/m) | – | 40 |
| Refractive index | 1.33 | 1.40 |

Table 2
Image-capturing conditions

| | $(x,y)$-plane | $(y,z)$-plane |
|---|---|---|
| Capturing rate (frame/s) | 48 | 85 |
| Pixel numbers | $1004 \times 1004$ | $1000 \times 248$ |
| Pixel resolution (mm$^2$) | $0.052 \times 0.052$ | $0.059 \times 0.059$ |
| Frame numbers per run | 1560 | 2560 |

was higher than the image-capturing rates shown in Table 2. Therefore, the particle was appropriate for the visualization of the turbulent swirling water flow.

## 4. Image capturing

The outside of the pipe in the test section was covered with transparent plates as shown in Fig. 3. The gap between these plates and the outer surface of the pipe was filled with water in order to reduce the deformation of the image through the pipe wall.

Green laser light was adopted as light source. The laser light was divided into two lines by a half mirror, and then each line was expanded by using cylindrical lenses to obtain light sheets. The two light sheets illuminated the test section from the opposite direction in one plane. When the velocity on a cross section (an $(x,y)$-plane) was measured, the light sheet illuminated the flow from above and below (see Fig. 3(a)). The width and thickness of the light sheet were 70 mm and 10 mm, respectively.

Fluorescence from the particles was captured by a progressive-scan CCD video camera (Basler, A202k) with an optical filter located at the downstream end of the pipe. The image-capturing condition is shown in Table 2. The captured images were recorded into a PC through a frame grabber. Note that the images of fluorescence from the tracer particles were larger than the sizes of the particles. In fact, the fluorescence was detected by at least four pixels. This was appropriate for the particle tracking velocimetry (hereafter called PTV).

When the velocity on a vertical plane parallel to the axis (a $(y,z)$-plane) was measured, the lenses were rotated 90 deg (see Fig. 3(b)). The width and thickness of the light sheet was 10 mm and 5 mm, respectively.

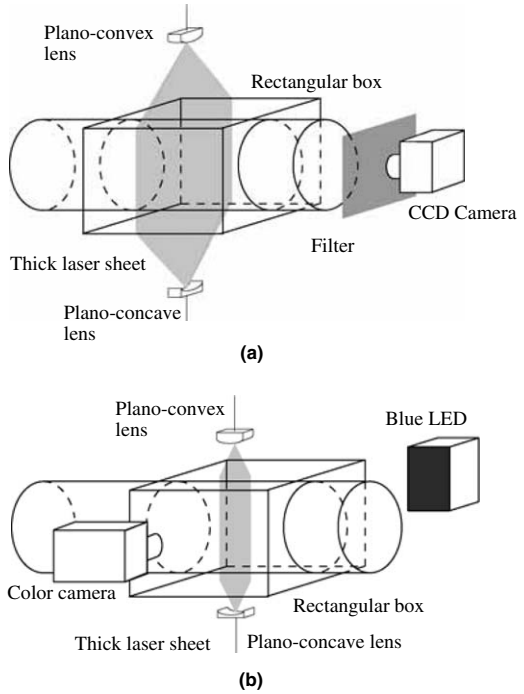


Fig. 3. Arrangement of optics and video camera: (a) axial view and (b) side view.

Since the phase interface was not identified clearly by using the laser light sheet only, we adopted the shadow image technique (hereafter called SIT) to obtain the phase interface. A blue LED array was placed beside the pipe as a backlight for SIT. Fluorescence from the tracer particles and the LED backlight were captured by a color CMOS camera (Silicon video 9M001C) located on the other side of the pipe. The image-capturing condition is shown in Table 2. The captured images were recorded into a PC through a frame grabber.

We carried out five runs of image capturing for the cross section of $z/D = 3.4$ and the $(y,z)$-plane at $x = 0$ around $z/D = 3.4$.

## 5. Image processing

The preprocessing for the images was the same as that adopted in our previous study (Kouda and Hagiwara, 2006). The PTV technique with the velocity gradient tensor method, which was developed by Ishikawa et al. (2000), was applied to the preprocessed images in order to obtain velocity vectors. First, the matrix including the velocity gradient tensor was calculated for pairs of neighboring particles in a specific region around a particle in this method. Secondly, the sum of the square of the errors was evaluated. Then, these procedures were applied to all the candidate particles until the sum took its minimum value. This method has the advantage of accurately reproducing velocity fields with strong deformation due to the rotational motion of flow.

All the velocities of the tracer particles were redistributed to the grid points of $38 \times 38$ in the $x$ and $y$ directions on the $(x,y)$-plane. The velocity of each particle was shifted to the nearest grid point in this redistribution procedure. Similarly, the velocities of the particles were redistributed to the grid points of $40 \times 1$ in the $y$ and $z$ directions on the $(y,z)$-plane.

The analysis for the uncertainty of the velocity was carried out. The uncertainty caused by the present image processing methods was estimated to be 1.0 mm/s for the maximum value of the azimuthal mean velocity of 136 mm/s on the $(x,y)$-plane. The uncertainty was estimated to be 2.0 mm/s for the maximum value of the streamwise mean velocity of 90 mm/s on the $(y,z)$-plane. These show that the measured velocity was accurate.

## 6. Results and discussion

### 6.1. Mean velocities in the azimuthal and radial directions

Fig. 4 shows the mean velocity vectors on the $(x,y)$-plane at $z/D = 3.4$ in the case without the droplets. The swirl is clearly seen in this figure. The center of the swirl is found to shift slightly in the positive direction of the $x$-axis. This is due to the meandering of the center of the swirl.

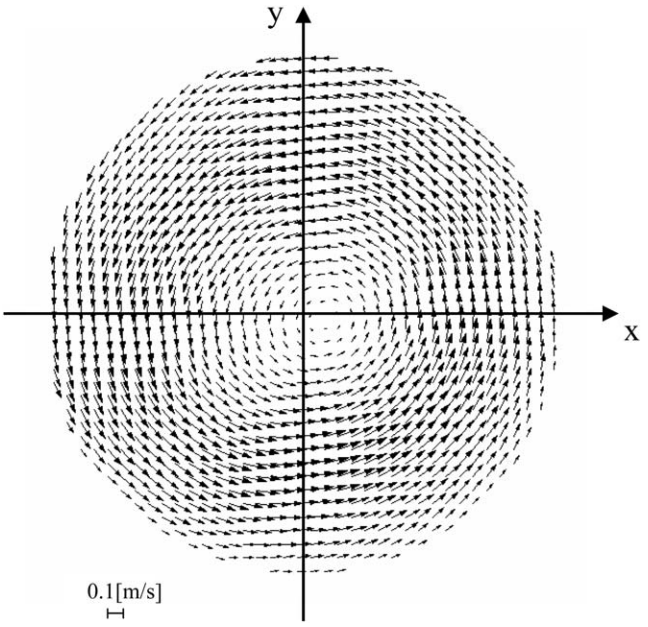


Fig. 4. Vector field of mean velocity at $z/D = 3.4$.

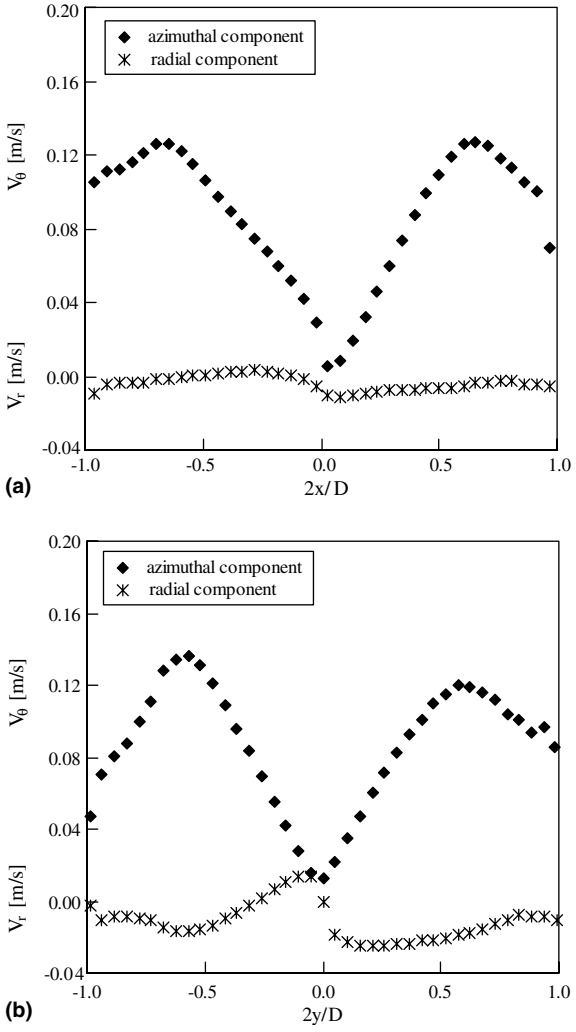


Fig. 5. Mean velocities in the azimuthal and radial directions: (a) along the horizontal axis and (b) along the vertical axis.

Fig. 5(a) and (b) depicts the profiles of azimuthal mean velocity, $V_\theta$, along the horizontal and vertical axes in the case without the droplets, respectively. It is found that this velocity increases almost linearly from zero near the axis with the absolute values of $x$ and $y$ in the regions of $-0.59 < 2x/D < 0.55$ and $-0.52 < 2y/D < 0.52$. This shows that the velocity field in the central region of $2r/D < 0.52$ is similar to that of a forced vortex.

The swirl number defined by Eq. (1) was 1.34 at the cross section. This is 2.9 times higher than the number in our previous study (Kouda and Hagiwara, 2006) in the case with the buoyancy-free droplets. Also, $V_{\theta\max}$ in Eq. (2), which was determined from the profiles in Fig. 5(b), is approximately 1.9 times higher than that in our previous study. This proves that the swirl in the present study is stronger than that in the previous study.

The profiles of radial mean velocity, $V_r$, along the horizontal and vertical axes are also shown in Fig. 5(a) and (b). $V_r$ takes slightly positive values in the regions of $-0.54 < 2x/D < -0.13$ and $-0.26 < 2y/D < -0.05$, and takes slightly negative values in the regions of $0 < 2x/D < 1$ and $0 < 2y/D < 1$. This shows that weak motion gathering into the pipe axis was superimposed on the swirl motion of the fluid. This is due to the wake flow of the boss (20 mm in diameter) of the impeller mentioned below. Therefore, the water in the test section had a spiral motion.

### 6.2. Diameter and motion of droplets

Fig. 6 indicates the total number of frames $N$, in which the droplets appeared, as a function of the droplet equivalent diameter, $d$. $N$ increases with the total number of droplets in flow. Two peaks are seen at $d = 4.0$, 6.1 mm in the region of $3.2 < d < 6.8$ mm. The Stokes number for the droplets was in the range of 2.5–10.

The distribution of droplet diameters resulted from the phase interactions at the outlets of the tubes and in the flow between the outlets and measuring location. First, we examine the phase interaction at the outlets of the tubes in order to understand the distribution shown in Fig. 6. The following forces act on the oil injecting from the tubes; (1) the pressure-gradient force towards the axis, (2) the azimuthal component of the drag force, (3) the radial component of the drag force, (4) the streamwise component of the drag force, (5) the buoyancy force and (6) the interfacial tension force at the peripheral of the tube. The first three forces are caused by the swirl motion, and the directions of these forces depend on the locations of the tubes. The directions of the fourth and fifth forces do not depend on the tube location. The magnitudes of all the forces, except for the interfacial tension force, increase with the volume of the oil at the tube outlet. The vectors of the first three forces and the buoyancy force at the tube outlets are shown

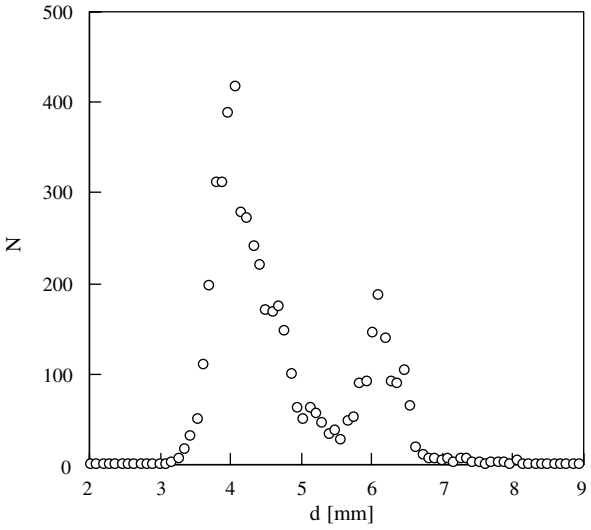


Fig. 6. Number of frames as a function of droplet equivalent diameter.

in Fig. 7. The magnitudes of the first three forces were estimated from the maximum among the four values of $V_\theta$ at $2r/D = 0.5$ in Fig. 5, the maximum among the four values of $V_r$ at $2r/D = 0.5$ in Fig. 5 and the maximum among the values of $V_z$ at $2r/D = 0.5$ mentioned below.

At the outlet of the top tube $(0, 0.25D, 2.3D)$, the direction of the buoyancy force is opposite to the directions of the pressure-gradient force and the radial component of the drag force. Thus, the net force in the vertical direction at this outlet is not strong. Furthermore, the azimuthal component of the drag force at the outlet is weaker than that at the other outlets, because the actual value of $V_\theta$ at the outlet is lower than the value of $V_\theta$ at $(0, -0.25D)$, as shown in Fig. 5. The oil clings to the outlet for a long period until the resultant force due to the first four forces exceeds the interfacial tension force. Therefore, the diameter of the droplets formed at the outlet is relatively large. Similarly, the direction of the buoyancy force and that of the azimuthal component of the drag force are opposite to each other at the outlet of the left tube $(-0.25D, 0, 2.3D)$ in Fig. 7. Therefore, the diameter of the droplets at this outlet is relatively large.

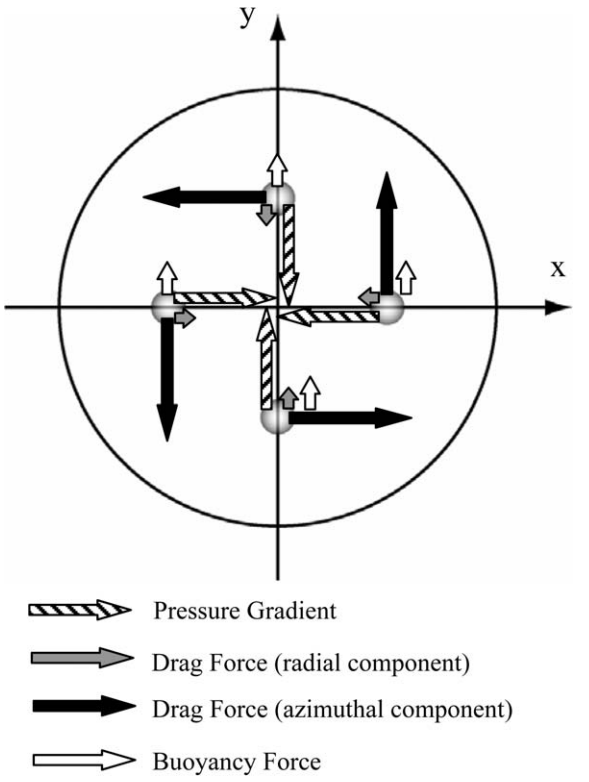


Fig. 7. Forces acting on oil at the outlets of tubes.

On the other hand, at the outlet of the bottom tube $(0, -0.25D, 2.3D)$, the directions of the buoyancy force, the pressure-gradient force and the radial component of the drag force are identical. Also, at the outlet of the right tube $(0.25D, 0, 2.3D)$ in Fig. 7, the directions of the buoyancy force and the azimuthal component of the drag force are upward, and the directions of the pressure-gradient force and the radial component of the drag force are identical. The net forces in the vertical direction at these outlets are strong. The oil clings to the outlets for a short period. Therefore, the diameters of the droplets formed at the outlets are relatively small. These dependencies of the droplet diameter on the location of the tube were confirmed by a supplemental experiment, in which the oil was injected only from one of the four tubes.

Next, we examine the phase interaction in the flow. Fig. 8 indicates $N$ as a function of $y$ at $x = 0$. Forty slots, whose width was $0.025D$, were defined in the $y$ direction, and the number for each slot was counted when the center of the droplet was in the slot. The numbers take more than half their maximum value in the region of $-0.43 < 2y/D < 0.43$. That is, many droplets were transported in the central region. This is clearly different from the result obtained in our previous study (Kouda and Hagiwara,

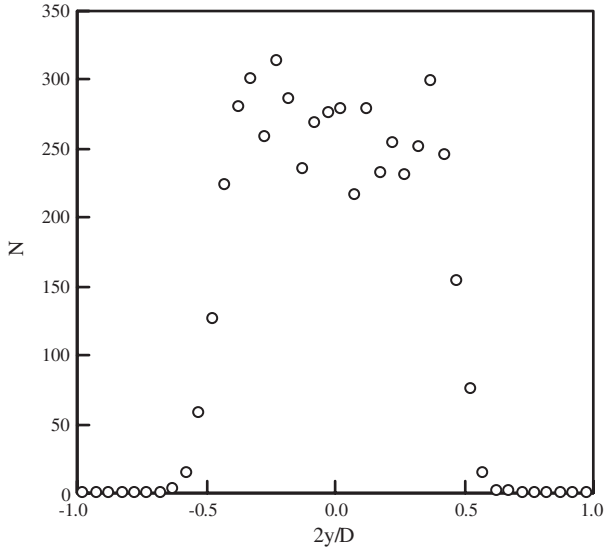


Fig. 8. Number of frames with droplet images as a function of vertical coordinate.

2006) in which many droplets were transported in the second quadrant region on the $(x, y)$-plane. (The downward component of $V_\theta$ balanced the upward velocity due to the buoyancy force in the case of weak swirl in our previous study.) In this sense, the strong swirl is effective in concentrating the low-density droplets into the central region.

### 6.3. Streamwise mean velocity

The profile of streamwise mean velocity on the plane of $x = 0$ in the case with the droplets and that in the case without the droplets are compared in Fig. 9. The decrease in the velocity is seen in the central region. This is due to the wake flow of the boss of the impeller. The difference in the profiles between the two cases is within the margin of error. This result is not the same as that in our previous study (Kouda and Hagiwara, 2006). Since the gradient of the $V_\theta$ in the present study is higher than that in our previous study, the droplet motion towards the axis due to the pressure-gradient force is more noticeable in the present study. The droplets moved to the streamwise direction have higher velocity than that of ambient fluid. This high velocity can be cancelled by the low velocity of wake flow by the droplets, which was originated at the detachment instant of the droplets from the tube outlets. Note that the droplets rotated around the pipe axis at least once by the swirl for the period they were being transported from the outlets of the tube to the measuring location.

### 6.4. Turbulence intensity in the streamwise direction

Fig. 10 shows the turbulence intensity in the streamwise direction in the case with the droplets and that without the droplets. It is found that the intensity in the case with the droplets is higher than that without the droplets in the region of $-0.53 < 2y/D < 0.48$. This region corresponds to the high value region of $N$ in Fig. 8. Thus, the enhancement of turbulence is the direct effect of the droplets. The

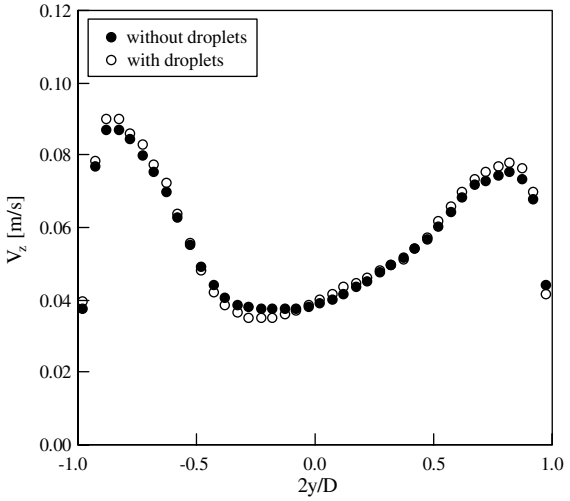


Fig. 9. Profiles of streamwise mean velocity.

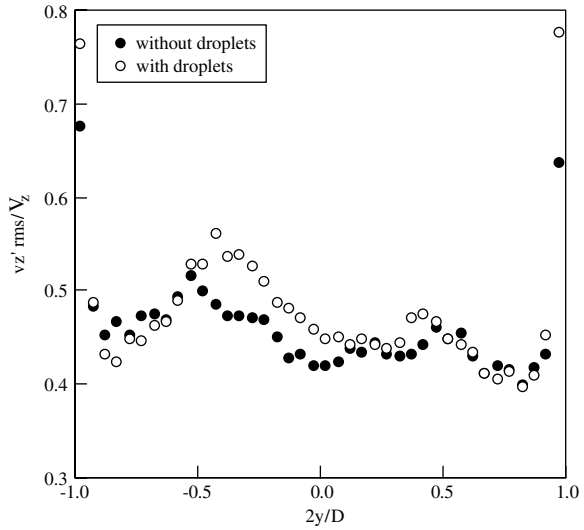


Fig. 10. Turbulence intensity in the streamwise direction.

increase in the intensity in the region of $-0.5 < 2y/D < 0$ is more noticeable than the other region. In this region, the directions of the pressure-gradient force and the buoyancy force acting on the droplets are upward (see Fig. 7). Thus, the relative motion of the droplets to the ambient fluid was intensified by these forces. Furthermore, the droplets can easily have relative motion to the water swirl motion because the Stokes number is higher than the unity mentioned above. For some typical droplets in the region, the Reynolds number based on the relative velocity between the droplet and the surrounding flow $v_{\mathrm{rel}}$, the droplet diameter $d$ and $\nu$, $Re_{\mathrm{d}} = v_{\mathrm{rel}} d/\nu$, was approximately equal to 150. According to the study on flow around the sphere carried out by Sakamoto and Haniu (1990), faint periodic motion is generated at the rear of the vortex-ring from behind the sphere in the case where $Re_{\mathrm{d}}$ is in the range of 130–300. Therefore, it can be thought that similar periodic motion occurs in the wake region of the droplets, and that it causes an increase in the intensity.

## 7. Conclusions

We carried out the measurement on the turbulent swirling water flow with the immiscible oil droplets in a horizontal pipe. The main conclusions obtained are as follows:

1. The distribution of droplet diameters had the twin peaks. The big droplets were generated by the long-term clinging of oil at the outlet of the oil injection tube. This is due to the force balance associated with the water swirl motion and the buoyancy.
2. The droplets in the central region moved in the streamwise direction due to the pressure-gradient force, the drag force and the buoyancy force. These droplets had higher velocity than the ambient water, and the wake flow of the droplets had lower velocity than the ambient water. Thus, the streamwise mean velocity of the water flow was not affected by the droplets.

3. It was thought that the faint periodic motion in the wake flow of some droplets caused the increase in the streamwise turbulence intensity.

## References

Hagiwara, Y., Takagaki, S., Yuge, T., 2003. Effects of a droplet on near-wall transport phenomena in turbulent downward liquid–liquid flow. J. Enhanc. Heat Transfer 10, 103–115.

Hagiwara, Y., Suzaki, T., Saegusa, D., 2005. Interaction between near-wall turbulence structure and immiscible droplets falling with wobbling motion in upward water flow. Energy 30 (2–4), 181–195.

Hjelmfelt Jr., A.T., Mockros, L.F., 1966. Motion of discrete particles in a turbulent fluid. Appl. Sci. Res. 16, 149–161.

Inaba, H., Horibe, A., Ozaki, K., Yokoyama, N., 1998. Liquid–liquid direct contact heat exchange using a perfluorocarbon liquid for waste heat recovery (Heat transfer characteristics obtained with perfluorocarbon droplets descending in a hot water medium). Trans. JSME 64B, 3838–3845 (in Japanese).

Ishikawa, M., Murai, Y., Wada, A., Iguchi, M., Okamoto, K., Yamamoto, F., 2000. A novel algorithm for particle tracking velocimetry using the velocity gradient tensor. Exp. Fluids 29, 519–531.

Jacobs, H.R., Golafshani, M., 1989. A heuristic evaluation of the governing mode of heat transfer in a liquid–liquid spray column. ASME J. Heat Transfer 111, 773–778.

Kaviany, M., 1994. Principles of Convective Heat Transfer. Springer-Verlag, New York (Section 6.1), pp. 417–425.

Kitoh, O., 1991. Experimental study of turbulent swirling flow in a straight pipe. J. Fluid Mech. 225, 445–479.

Kouda, T., Hagiwara, Y., 2006. Turbulent swirling water flow with oil droplets. Multiphase Sci. Technol. 18 (1), 55–72.

Lee, J.M., 1987. Drop size formations in agitating system. In: Cheremisinoff, N.P. (Ed.), Encyclopedia of Fluid Mechanics, vol. 6. Gulf Pub. Co., Houston, pp. 141–165 (Chapter 5).

Magaud, F., Nijafi, A.F., Angilella, J.R., Souhar, M., 2003. Modeling and qualitative experiments on swirling bubbly flows: single bubble with Rossby number of order 1''. ASME J. Fluids Eng. 125, 239–246.

Mitrovic, J., Stephan, K., 1996. Mean fluid temperatures in direct contact heat exchangers without phase change. Int. J. Heat Mass Transfer 39, 2745–2750.

Sakamoto, H., Haniu, H., 1990. A study on vortex shedding from spheres in a uniform flow. ASME J. Fluids Eng. 112, 386–392.

Satake, S., Kunugi, T., 1998. Direct numerical simulation of turbulent pipe flow. Trans. JSME 64B, 65–70 (in Japanese).

Tanaka, Y., Oba, G., Hagiwara, Y., 2003. Experimental study on the interaction between large scale vortices and particles in liquid–solid two-phase flow. Int. J. Multiphase Flow 29, 361–373.